Should virus capsids assemble perfectly? A simple equilibrium model for defects

Justin Spiriti, James Conway, Daniel M. Zuckerman

June 26, 2019

1 Abstract

Although published structural models of virus capsids generally exhibit a high degree of structural regularity or symmetry, structural defects might be expected for several reasons: the finite-temperature, fluctuating environment in which capsids assemble, the maturaton process many capsids undergo, and the requirement of some capsids for disassembly prior to genome delivery. Different lines of evidence also suggest the presence of defects: the observation of defective structures in computer simulations, and the presence of imperfect and off-pathway capsids in single-particle cryoEM studies. To begin to quantify the conditions under which defects might be expected, we extend prior work by developing a simple equilibrium theory for capsids based on a lattice model allowing for both ideal and defective sites. Both analytical and numerical calculations with the model show there is a fairly sharp threshold value for the difference in effective pair-binding affinities between ideally oriented and mixed ideal/defective pairs: below this capsid-specific threshold, there is an appreciable population of defective capsids. Even when defective sites are not allowed, there is generally some population of vacancies. Beyond furthering our understanding of potential structural heterogeneity in virus capsids, the findings suggest a novel strategy for assembly inhibition by enhancing 'off-lattice' interactions among capsid proteins via adaptor molecules.

2 Introduction

The assembly of the viral capsid is a critical step in the life cycle of all viruses [1, 2]. During each infection cycle, capsids must assemble for each new viral replicate before it leaves the cell, and often must go through maturation steps that involve significant changes in conformation as well. One consequence of the dynamic and intrinsically stochastic nature of viral capsid assembly may be that it does not always proceed to a precise end point and that occasionally defective capsids form. For example, there are three forms of the herpesvirus capsid, two of which do not correpsond to fully infectious viral capsids.[3, 4] The human hepatitis B viral capsid can assemble in vivo into either T=3 structures (with 90 subunit subunits per capsid) or T=4 structures (with 120 subunits per capsid); which structure forms appears to depend on the conformational behavior of seven amino acid residues on the C-terminal region of the HBcAg capsid subunit.[5–7] The nature of the structures that form may also depend strongly on the ambient conditions. For example, the cowpea chlorotic mosaic virus (CCMV) can form a variety of structures, including multiwalled shells, tubes, and "rosettes", depending on the pH and ionic strength.[8]

The limitations of conventional structural biology techniques make it very difficult to verify the formation of defective capsid structures directly. While structures of individual viral capsid subunits can be obtained by X-ray crystallography, most structures of complete capsids are obtained using cryoelectron microscopy (cryo-EM).[9, 10] Cryo-EM images often include capsids that are distorted or incomplete, or which have additional layers of subunits (fig. 1).[11] However, the resolution of individual cryo-EM images is low, so obtaining atomistic structures requires collecting, filtering, re-orienting and averaging many such images.[12–15] This in turn requires discarding images of capsids that appear to be defective, and exploiting symmetry in the averaging process, which artificially imposes a corresponding symmetry on the resulting structure. Since defective capsids are not uniform, this method cannot be applied to calculate high resolution structures of

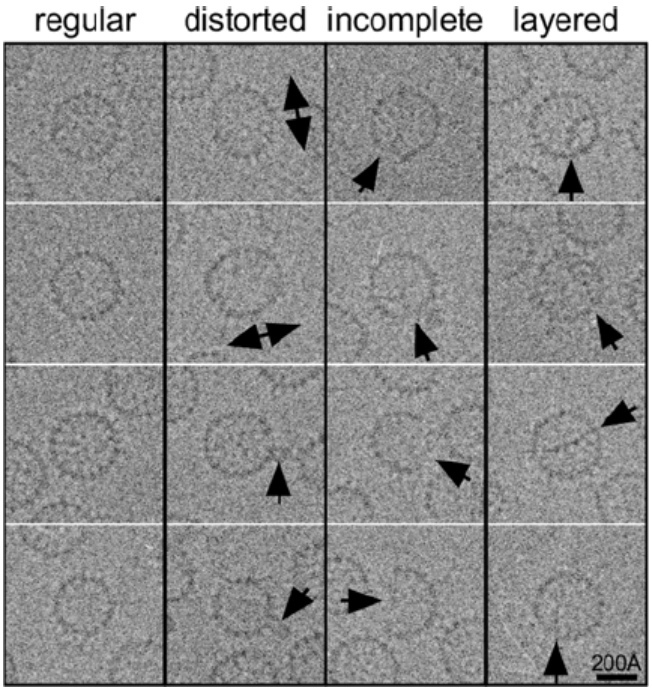

Figure 1: Heterogeneity in raw cryoEM data. Selected cryoEM images of hepatitis B capsid particles. Arrows indicate structural variation.

defective capsids. Similarly, X-ray crystallography exploits the perfect repetition of the crystal lattice thus excluding observation of irregular or infrequent capsids resulting from defects in assembly.

Computer simulations can enable detailed examinations of the mechanism of capsid assembly and the types of structures that can form.[16–20] Several simulations produced unusual, malformed structures, such as oblate capsids lacking icosahedral symmetry or aggregates composed of several partially formed capsids joined together in an irregular fashion.[21–24] In particular, a recent study of the assembly of the T=4 form of the hepatitis B viral capsid using a semi-atomistic model yielded trajectories with persistent defects, despite that a defect-free fully symmetric structure was the lowest energy conformation.[25]

Defective capsid formation can also be studied from a more fundamental perspective, focusing on thermodynamics and kinetics. One early model of equilibrium capsid assembly was based on a simplified representation of the capsid, in which 12 pentagonal subunits unite to form a dodecahedron, and a single, minimum-energy pathway for assembly. This model indicated that, for a range of plausible concentrations of free subunits, the concentration of intermediates was very low compared to that of either free subunits or complete capsids.[26] However, capsid subunits were considered rigid and able to exist in only two states: either fully attached to the capsid, or completely detached from it. Consequently, the only possible defects were vacancies. In addition, the assumption of a single minimum-energy pathway breaks down for large viruses because of the increased complexity of the structure and the larger number of sites where a subunit can be attached to a growing capsid. Other approaches focus on the maturation that many viral capsids undergo after initial assembly. This maturation involves the relaxation of elastic strains created by conformational changes within the subunits, and can be described by applying continuum elastic theory.[27]

In later work, extensive experimental studies of the thermodynamics and kinetics of hepatitis B viral capsid assembly were performed, using size exclusion chromatography to observe the concentrations of isolated subunits and complete capsids over time under different conditions. This data was then incorporated into a simplified thermodynamic-kinetic model for the assembly process.[26, 28, 29] Because significant concentrations of species with molecular masses intermediate between individual subunits and complete capsids were not observed, these studies suggest that capsid assembly can be considered a two-state process in which only free subunits or complete capsids exist in significant concentrations, depending on whether capsid formation is thermodynamically favored or not. However, the resolution of size exclusion chromatography and light

scattering as mass-measurement techniques is insufficient to distinguish between complete, perfect capsids and those that have small defects or vacancies. This work has had a significant influence on future theory regarding capsid assembly.[1, 2] Presaging some of our current work, a statistical mechanical lattice model has been developed for the assembly of the cowpea chlorotic mottle virus (CCMV) that could be used to study the thermodynamics of capsid assembly as a function of ionic strength and temperature.[30, 31]

In the work presented here, we also choose to work with the hepatitis B virus (HBV) capsid as a demonstration system, because of our cryo-EM images of this capsid which show a vairety of defects. Some of the defects represented include distorted, non-spherical capsids; incomplete capsids with gaps in their surface; and layered capsids with subunits forming additional surfaces inside an otherwise fully-formed capsid. Several instances of these defects are shown in figure 1.

We take a statistical-mechanical approach to the problem of determining the equilibrium distribution of capsid states. Our model is similar to the lattice gas model for studying phase transitions in critical fluids,[32, 33] but defined on a contact graph that reflects the geometry of the hepatitis B virus (HBV) capsid. The model incorporates the possibility of capsid subunits being partially attached or being in a conformational state such that their interactions with a partially formed capsid are not as strong as the intersubunit interactions in a fully formed capsid. The model can be solved analytically under the approximation that defects in capsids are isolated, and can also be simulated numerically using the Metropolis Monte Carlo method.[34]

Using this model, we characterize the conditions under which capsid formation is thermodynamically stable, as a function of the chemical potential of free capsids and the different interaction strengths. We show that the proportion of defective capsids can be appreciable when the difference in strengths between ideal and defective subunit interactions is below a threshold. We further extend the analysis to other viruses by considering the relationship between this threshold, the number of subunits in a capsid, and the number of contacts each subunit makes. These results suggest that defective capsids can form in significant concentrations under a range of conditions.

3 Materials and Methods

3.1 Model for capsid formation

We construct a statistical-mechanical model for capsid assembly, first defining the possible discrete states of the model and writing an energy function that determines the free energy of each possible state, given the parameters of the model. The equilibrium behavior of the model then depends only on this energy function, and the laws of statistical mechanics give the distribution of possible states for the model. Given a constant chemical potential for free subunits, we can determine the distribution of sizes of partially formed capsids. Since there is no equation of motion for the system, we do not obtain dynamics or predict kinetics of capsid assembly using this model.

Physically, each discrete state of our model represents a *set* of continuum configurations in the underlying configuration space. Therefore, all state energies are intrinsically *free* energies that account for both energetic and entropic characteristics of the underlying configurational sub-ensembles [35]. We emphasize that, in this work, we are not estimating the free-energetic parameters of the model, but rather exploring the consequences of a physically plausible range of parameter choices.

We employ a simple lattice-like graphical model with N sites (fig. 2), in which each site i can be in one of three states: unoccupied, "ideally" occupied (i.e. in the orientation suitable for the symmetric capsid), or mis-occupied (i.e. occupied but mis-oriented compared to the symmetric configuration). A contact graph $\mathcal{G}$ (fig. 2) shows which sites interact with each other. Thus the free energy of a capsid configuration $\mathbf{x}$ is given by

$$G(\mathbf{x}) = \sum_{\text{edges } ij \in \mathcal{G}} \Delta G_{\text{int}}(x_i, x_j) \tag{1}$$

where $\Delta G_{\text{int}}(x_i, x_j)$ is an interaction free energy that depends on the occupation states x_i and x_j of the two sites i and j.

The interaction energy ΔG_{int} can take on one of three possible values: ΔG_{ideal}, for interactions between ideally occupied sites, ΔG_{mixed} for interactions between a ideally occupied site and a mis-occupied site,

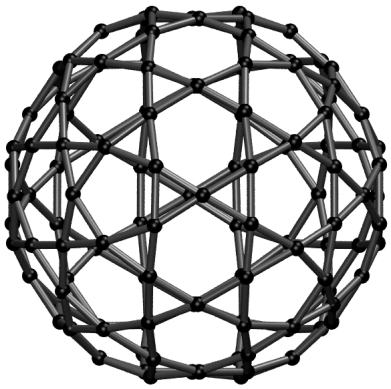

(a)

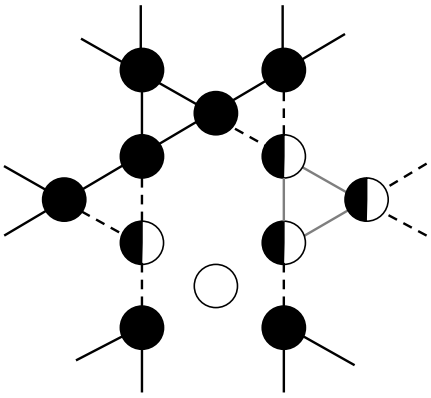

(b)

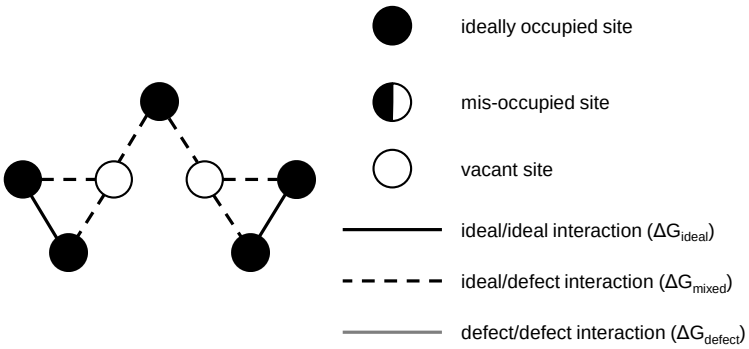

(c)

Figure 2: Lattice model for Hepatitis B virus capsid. (a) The perfect capsid, with all sites ideally occupied. (b) F showing ideally occupied sites (black circles), mis-occupied sites (black half-circles), and vacant sites (white circles). The interaction energy between ideally occupied sites or between mis-occupied sites is ΔG_{ideal} (solid line), whereas the interaction energy between an ideally occupied and a mis-occupied site is ΔG_{mixed} (dotted line). (c) Diagram of a defect in a capsid, consisting of two neighboring vacant sites surrounded by occupied sites.

or ΔG_{defect} for interactions between mis-occupied sites. In general, we expect that interactions between ideally occupied and mis-occupied sites will be weaker than those between ideally occupied sites. We defined the difference $\Delta\Delta G$ to be the absolute difference between the two interaction energies. (For example, for $\Delta G_{\text{ideal}} = -5.0k_BT$ and $\Delta G_{\text{mixed}} = -2.0k_BT$, $\Delta\Delta G$ would be $3.0k_BT$.) We also assumed that the interaction between two adjacent mis-occupied sites (ΔG_{defect}) would have the same strength as that between ideally occupied sites (ΔG_{ideal}). Note that all of these interaction energies account for average effects of configurational fluctuations and hence represent effective free energies. Several examples of possible states for the model are shown in figure 2.

The probability of any given configuration $\mathbf{x}$ can be calculated based on its energy. In the canonical ensemble (constant temperature and number of particles), the probability of any particular contribution of energy $G(\mathbf{x})$ is given by the Boltzmann distribution:

$$p(\mathbf{x}) \propto \exp[-\beta G(\mathbf{x})] \tag{2}$$

Since the total number of occupied sites is fixed, this must be normalized in such a way that the sum of the probabilities of all configurations with N occupied sites is equal to 1. This gives the expression

$$p(\mathbf{x}) = \frac{\exp[-\beta G(\mathbf{x})]}{\sum_{\text{configs } N(\mathbf{x})=N} \exp[-\beta G(\mathbf{x})]} \tag{3}$$

where the sum in the denominator is taken over all configurations having N occupied sites, and where $\beta = 1/k_B T$ with T being the temperature of the system.

However, in order to be able to study the distribution of the number of occupied sites, we choose to work in the grand canonical ensemble, in which the number of particles is assumed to vary and their chemical potential (designated μ) is assumed to be constant. This corresponds to considering the partially-formed capsid is treated as being in equilibrium with an ideal solution of free subunits. The chemical potential μ is related to the concentration of subunits in the surrounding bath by the following relation:

$$\mu = k_B T \ln \frac{[\text{subunit}]}{[\text{subunit}]_{\text{ref}}} \tag{4}$$

The probability of a given configuration $\mathbf{x}$ is then given by

$$p(\mathbf{x}) \propto \exp[-\beta G(\mathbf{x})] \exp[-\beta \mu N(\mathbf{x})] = \exp\{-\beta[G(\mathbf{x}) - \mu N(\mathbf{x})]\} \tag{5}$$

where $N(\mathbf{x})$ is the number of occupied sites for configuration $\mathbf{x}$. As with the canonical ensemble, it is necessary to normalize this to ensure that the total probability of all configurations is equal to 1. This gives

$$p(\mathbf{x}) = \frac{\exp\{-\beta[G(\mathbf{x}) - \mu N(\mathbf{x})]\}}{\sum_{\text{all configs}} \exp\{-\beta[G(\mathbf{x}) - \mu N(\mathbf{x})]\}} \tag{6}$$

where the sum now covers all possible configurations regardless of number of occupied sites. The denominator is the grand canonical partition function Ξ. We assume that both fully and mis-occupied sites have the same chemical potential, so that the total includes both types of sites. The total probability of having N subunits in the capsid is given by summing the above probability over all configurations having N occupied sites:

$$p(N) = \frac{\sum_{\text{configs } N(\mathbf{x})=N} \exp\{-\beta[G(\mathbf{x}) - \mu N(\mathbf{x})]\}}{\sum_{\text{all configs}} \exp\{-\beta[G(\mathbf{x}) - \mu N(\mathbf{x})]\}} \tag{7}$$

3.2 Approximate analytical approach based on assuming isolated defects

It is possible to obtain an analytical expression for the partition function of this model if we make the approximation that all defects (either empty sites or mis-occupied sites) are isolated from each other. This is a good approximation if there are few defects, which is the regime of primary interest to us, since we are interested in situations in which capsids are generally stable.

For a capsid with N sites in total, each of which has k nearest neighbors, there are a total of $Nk/2$ contacts between sites. Therefore, the energy of a structurally perfect capsid is given by

$$G_{\text{perfect capsid}} = -N\mu + \frac{Nk}{2} \Delta G_{\text{ideal}} \tag{8}$$

If one site is changed to an empty site, this removes the interactions along k edges, so the energy and its difference from the perfect capsid are given by

$$G_{\text{one vacant site}} = -(N-1)\mu + \left(\frac{Nk}{2} - k\right) \Delta G_{\text{ideal}} \tag{9}$$

$$\Delta G_v = G_{\text{one vacant site}} - G_{\text{perfect capsid}} = \mu - k \Delta G_{\text{ideal}} \tag{10}$$

If instead we change one site to a mis-occupied site the energy and its difference are given by

$$G_{\text{one mis-occupied site}} = -N\mu + \left(\frac{Nk}{2} - k\right)\Delta G_{\text{ideal}} - k\Delta G_{\text{mixed}} \tag{11}$$

$$\Delta G_m = G_{\text{one mis-occupied site}} - G_{\text{perfect capsid}} = k\Delta G_{\text{ideal}} - k\Delta G_{\text{mixed}} = -k\Delta\Delta G \tag{12}$$

where we have defined the interaction energy difference $\Delta\Delta G = \Delta G_{\text{mixed}} - \Delta G_{\text{ideal}}$.)This is consistent with the above definition of $\Delta\Delta G$ when both ΔG_{ideal} and $\Delta G_{\text{mixed}} \leq 0$. Also, the chemical potential term does not change because we are assuming the chemical potential of mis-occupied sites to be the same as ideally occupied sites.)

If we assume that all sites are isolated then the number of configurations with N_v empty sites and N_m mis-occupied sites is $\frac{N!}{N_v!N_m!(N-N_v-N_m)!}$. The difference in energy of each of these configurations from the perfect capsid is given by

$$\Delta U = N_v\Delta G_v + N_m\Delta G_m \tag{13}$$

It follows that the grand canonical partition function for this model is given by

$$\Xi = \exp[-G_{\text{perfect capsid}}] \sum_{N_v,N_m=0}^{N} \frac{N!}{N_v!N_m!(N-N_v-N_m)!} \exp[-N_v\Delta G_v - N_m\Delta G_m] \tag{14}$$

If we define $z_v = \exp[-\Delta G_v]$ and $z_m = \exp[-\Delta G_m]$ then we can see that this sum is a multinomial expansion, and so we can sum it analytically.

$$\Xi = \exp[-G_{\text{perfect capsid}}] \sum_{N_v,N_m=0}^{N} \frac{N!}{N_v!N_m!(N-N_v-N_m)!} z_v^{N_v} z_m^{N_m} \tag{15}$$

$$= \exp[-G_{\text{perfect capsid}}] \left(1 + z_v + z_m\right)^N \tag{16}$$

Since there is only one perfect capsid configuration, its probability is given by

$$p_{\text{perfect capsid}} = \frac{\exp[-G_{\text{perfect capsid}}]}{\Xi} = \frac{1}{(1+z_v+z_m)^N} = \frac{1}{(1+\exp[-(\mu - k\Delta G_{\text{ideal}})] + \exp[-k\Delta\Delta G])^N} \tag{17}$$

A plot of this expression is given in figure S3a in the Supporting Information.

3.3 Application to the hepatits B virus capsid

We apply the lattice model to study the HBV capsid through its contact graph. The capsid is composed of 120 dimers, each of which consists of a pair of subunits, each contributing a pair of helices to the 4-helix bundle interface and furhter linked by a disulfide bridge. We considered each dimer to constitute a site in our model. We constructed the contact graph $\mathcal{G}$ for the virus from the structure of the capsid given in the PDB (code 1QGT)[36] by including an edge for each pair of dimers in which there is at least one pair of α carbons within 10 Å of each other in the complete structure of the capsid. In this graph there are 4 nearest neighbors for each site.

Given a specific contact graph $\mathcal{G}$, the approximate analytical approach of the previous section may be extended to incorporate defects that are not isolated. For example, in the hepatitis B capsid, of the $120!/(2!\,118!) = 7140$ configurations with exactly two empty sites, 240 have the sites touching each other. The difference in energy between these configurations and the perfect capsid is $2\mu - 7\Delta G_{\text{ideal}}$, not $2\mu - 8\Delta G_{\text{ideal}}$, which would be the energy difference associated with two isolated empty sites. This is because a defect of this type removes the interactions among only seven edges rather than eight (see figure 2c. Thus the correction to Ξ needed to account for defects of this type is given by

$$\frac{\Xi}{\exp[-U_{\text{perfect capsid}}]} = (1+z_v+z_m)^{120} - 240z_v^2(1+z_v+z_m)^{113} + 240\exp[-(2\mu - 7\Delta G_{\text{ideal}})](1+z_v+z_m)^{113} \tag{18}$$

$$= (1+z_v+z_m)^{120} - 240z_v^2[\exp(-\Delta G_{\text{ideal}}) - 1](1+z_v+z_m)^{113} \tag{19}$$

where the second term in the first line subtracts out the incorrect terms in Ξ and the third term replaces them with the correct terms. The factor of $(1 + z_v + z_m)^{113}$ accounts for the possibility of isolated defects among the 113 sites not occupied by or touching the two empty sites that are together. In addition to this, two other correction terms in $z_v z_m$ and z_m^2 would be needed to account for defects in which one of the touching sites was partially attached and the other empty, or both partially attached. Additional terms in higher powers of z_v or z_m would be needed for defects involving three or more sites touching each other.

This approach is very reminiscent of the well-known virial expansion,[32, 33], where the effect of intermolecular forces in a real gas can be expressed as correction terms in powers of the density, relative to the partition function of an ideal gas. These correction terms can be determined using cluster diagrams. For viruses, the correction terms depend on the details of the contact graph and the particular defects that are possible, and can be derived in a similar manner to the example given above.

3.4 Monte Carlo simulations

One way to produce configurations with the distribution given by equation 6 is by performing what is known as a Metropolis Monte Carlo simulation. In this computational technique, we perform moves which change the system from one configuration to another. These moves are accepted with probability $\min(1, \exp[-\beta \Delta H(\mathbf{x})])$ where $H(\mathbf{x})$ is the Hamiltonian defined by

$$H(\mathbf{x}) = G(\mathbf{x}) - \mu N(\mathbf{x}) = -\mu N(\mathbf{x}) + \sum_{\text{edges } ij \in \mathcal{G}} \Delta G_{\text{int}}(x_i, x_j) \tag{20}$$

where N is the total number of subunits and ΔH is the change in H in going from an old to a new configuration.

We performed a set of Monte Carlo simulations for our model as applied to the hepatitis B capsid, using the contact graph $\mathcal{G}$ constructed from its structure as described above. Monte Carlo simulations of the model were performed with varying values of μ, ΔG_{ideal}, and ΔG_{mixed} to map out a "phase diagram" for the system. The Monte Carlo moves for these simulations consisted of choosing a site i at random and changing its state. Each simulation lasted for 1 billion trial moves, and the average number and distribution of the number of occupied sites were computed. The simulations were performed on a grid in μ-ΔG_{ideal}-ΔG_{mixed} space in which μ ranged from $-6k_BT$ to $6k_BT$ in steps of $0.2k_BT$, ΔG_{ideal} ranged from $-5k_BT$ to 0 in steps of $0.25k_BT$, and ΔG_{mixed} ranged from ΔG_{ideal} to 0 in steps of $0.25k_BT$. Only simulations in which $|\Delta G_{\text{mixed}}| \leq |\Delta G_{\text{ideal}}|$ were run.

To be considered a "partially formed capsid," a collection of subunits must be touching each other, so that they would be expected to move together because of the forces holding them together, but independently of any other collection of subunits. Consequently, for the purposes of analyzing this simulation, a "partially formed capsid" was defined as a set of occupied sites (either ideally occupied or mis-occupied) that span a connected subgraph of the contact graph $\mathcal{G}$. Therefore, after each trial move of the simulation, the subgraph of $\mathcal{G}$ spanned by the occupied sites was determined and divided into connected components. The distribution of the sizes of these subcomponents was then used for further analysis. The probability of perfect capsids (in which every site is ideally occupied) was determined separately.

4 Results

We present results from both Monte Carlo simulations and our analytical approximation, noting that the latter readily extends to arbitrary spherical capsids. We study the average and distribution of the sizes of partially formed capsids and the fraction of perfect capsids as a function of the three parameters of our model: μ, the chemical potential of free dimers with which the capsid is in equilibrium; ΔG_{ideal}, the strength of the interaction between ideally occupied sites; and ΔG_{mixed}, the strength of the interaction between an ideally occupied and a mis-occupied site. We compare these results to those from our analytical approach, which relies on the approximation that defects are isolated and therefore is expected to work best when capsid formation is strongly favored and only occasional defects still occur. We then extend the predictions of the analytical model to other spherical capsid viruses.

4.1 Structural heterogeneity in the hepatitis B viral capsid model

We first confirm that the average number of occupied sites depends on μ and ΔG_{ideal} (for $\Delta\Delta G = 0$) as expected. Figure 3 indicates that capsid formation is more favorable for a higher μ (implying a higher concentration of free subunits in equilibrium with the capsids) and for higher ΔG_{ideal} (stronger interactions between subunits). Similar plots with other values of $\Delta\Delta G$ (shown in figure S1 in the Supporting Information) were very similar to the plot shown in figure 3, implying that the average number of occupied sites does not vary much with $\Delta\Delta G$.

The model makes predictions regarding structural heterogeneity. Figure 4 shows the actual distribution of the number of occupied sites for selected points in the $(\mu, \Delta G_{\text{ideal}})$ plane. Most importantly, there is always some population of imperfect capsids, and this becomes dominant in some regions of parameter space. It is clear that, while the average number of occupied sites depends only weakly on $\Delta\Delta G$, the actual distributon of capsid sizes can vary significantly. For the points shown, the distributions have two peaks, one corresponding to a nearly fully formed capsid, the other corresponding to an isolated subunit. The probability minimum between these peaks increases with $\Delta\Delta G$. This is probably because of entropic effects. Adding a third state increases the number of possible configurations, and in particular for larger capsids, there are more ways to mix occupied

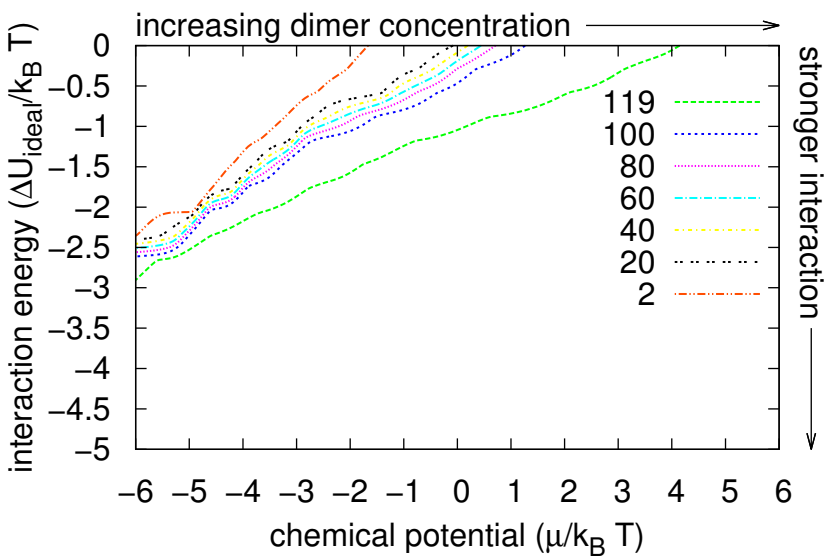

Figure 3: Dependence of capsid formation on chemical potential μ and interaction strength ΔG_{ideal}. Contour plot of the average connected capsid size (including mis-occupied sites) in Monte Carlo simulations of our model on the hepatitis B virus contact graph in the $(\mu, \Delta G_{\text{ideal}})$ plane for $\Delta\Delta G = 0$. Plots for other values of $\Delta\Delta G$ are found in figure S1 of the Supporting Information. Note that for ideal solutions $\Delta\mu \sim -k_B T \ln[\text{dimer}]$. Higher concentration and stronger interactions lead to more fully formed capsids.

When do structurally perfect capsids predominate? We studied the proportion of perfect capsids, where all sites had to be ideally occupied, and compared results from the Monte Carlo simulations to the analytical results obtained using the isolated-defects approximation (eq. 17). Figure 5 shows this proportion as a function of μ, ΔG_{ideal}, and ΔG_{mixed}, with plots in the $(\Delta G_{\text{ideal}}, \Delta G_{\text{mixed}})$ plane. The proportion of perfect capsids depends strongly on $\Delta\Delta G = |\Delta G_{\text{ideal}}| - |\Delta G_{\text{mixed}}|$, and shows a critical threshold of $\Delta\Delta G \approx 2.5 k_B T$. Above this threshold, and for a sufficient interaction strength, structurally perfect capsids predominate, while below this threshold, the fraction of defective capsids can become significant. As $\Delta\Delta G$ approaches zero, the many imperfect but complete capsid configurations in which some sites are mis-occupied, but no sites are vacant, come to have the same energy, and therefore the same probability, as the one perfect capsid

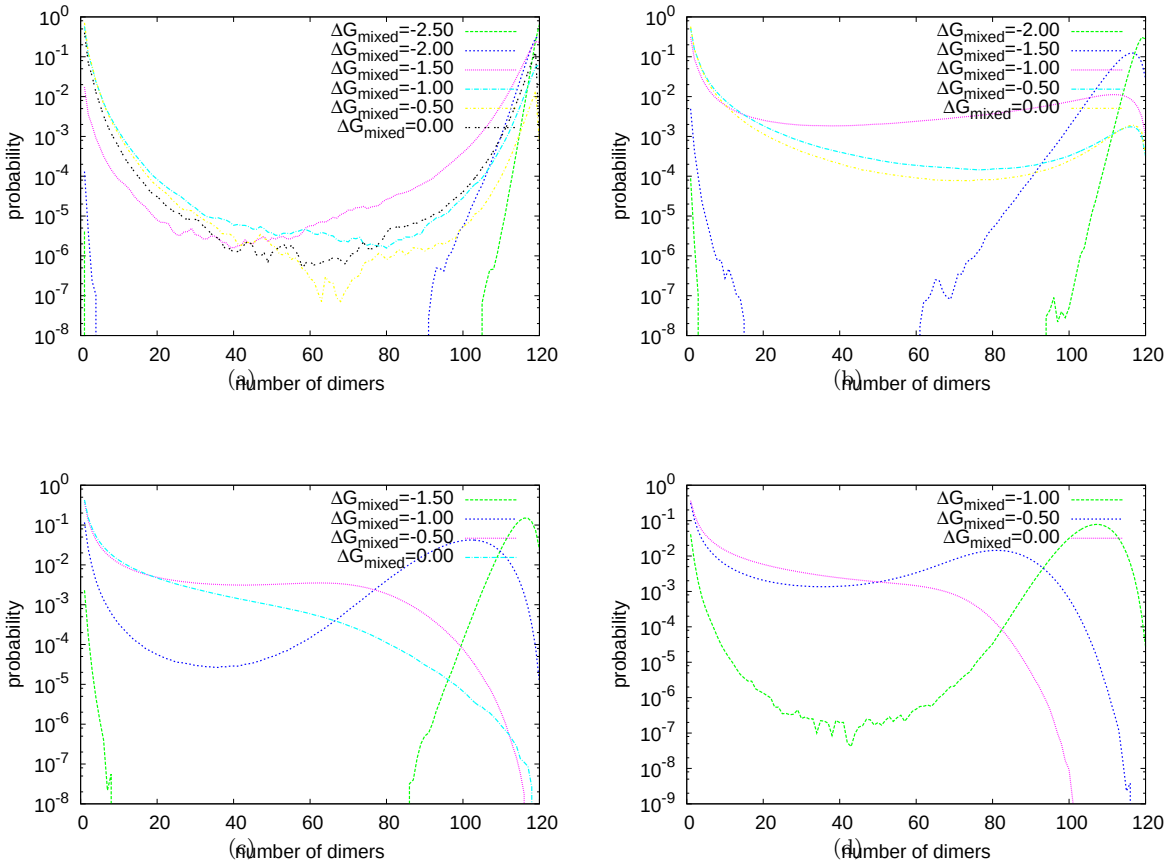

Figure 4: Effect of defective sites on the distribution of partial capsid sizes. Distribution of the connected capsid size as a function of ΔG_{mixed} for selected points in the $(\mu, \Delta G_{\text{ideal}})$ plane. Points were chosen where the distribution of capsid sizes showed two peaks corresponding to nearly-complete capsids and isolated dimers. (a) $(\mu, \Delta G_{\text{ideal}}) = (-5.0, -2.5)$; (b) $(\mu, \Delta G_{\text{ideal}}) = (-4.0, -2.0)$; (c) $(\mu, \Delta G_{\text{ideal}}) = (-3.0, -1.5)$; (d) $(\mu, \Delta G_{\text{ideal}}) = (-2.0, -1.0)$. Once $\Delta\Delta G \gtrsim 1k_BT$, there is an appreciable population of partially formed capsids and even a depletion of full capsids for weaker interaction strengths.

configuration in which all sites are ideally occupied. Consequently, the distribution of configurations is dominated by imperfect capsids for entropic reasons, and the probability of a perfect capsid is infinitesimally small for $\Delta\Delta G = 0$. The threshold of $2.5k_BT$ represents the point at which the lower energy of a ideally occupied site outweighs this entropic effect. The plots of results from the Monte Carlo simulations are qualitatively similar to the analytical results. However, there seem to be differences for large values of $\Delta\Delta G$, presumably due to defects involving neighboring partially-attached subunits.

The value of ΔG_{defect} has little impact on the probability of perfect capsids, as demonstrated by plots of the perfect capsid probability for various values of ΔG_{defect}, as shown in figure S4 in the Supporting Information. Because it is the interaction energy between adjacent mis-occupied sites, it cannot appear in an analytical approximation that assumes that all the defects are isolated. It would appear in second-order and higher terms in the virial expansion corresponding to defects in which two mis-occupied sites are adjacent to each other.

4.2 Model prediction for arbitrary spherical capsids

We extended our analysis to arbitrary spherical viral capsids using equation 17, a mathematical relationship between N and k, which are the geometric properties of a viral capsid, and the energy difference $\Delta\Delta G$

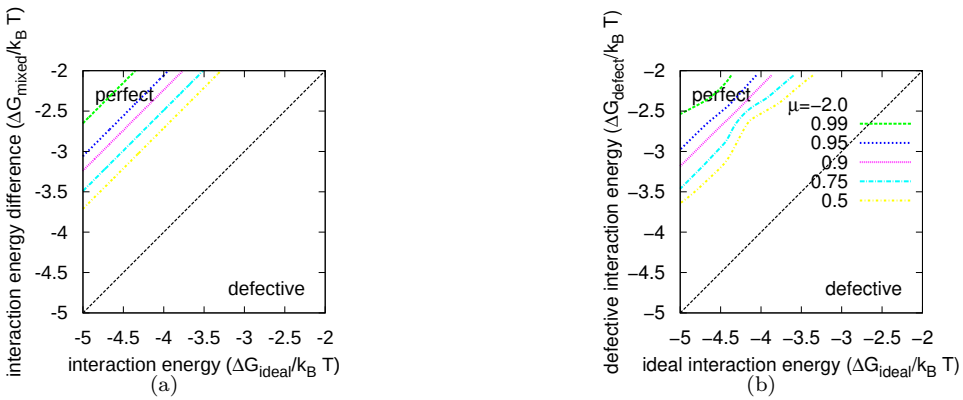

Figure 5: When are perfect capsids expected? (a) Plot of $p_{\text{perfect capsid}}$ as determined from equation 17 and (b) $p_{\text{perfectcapsid}}$, as determined from MC simulations, both showing the position of the 0.99 contour in the $(\Delta G_{\text{ideal}}, \Delta G_{\text{mixed}})$ plane (chemical potential and ideal interaction energy) for $\mu = -2.0 k_B T$.

needed for the formation of defective capsids. Under the conditions under which capsid formation is favored, μ is large and positive and there are strong interactions between ideally occupied sites; consequently, the term $\exp[-(\mu - k\Delta G_{\text{ideal}})]$ is relatively small. If we approximate the expression further by dropping this term and invert the remaining equation in terms of $\Delta\Delta G$ we obtain an expression for the threshold value of $\Delta\Delta G$ below which the proportion of defective capsids exceeds a specified threshold.

$$\Delta\Delta G = -\frac{1}{k} \log \left(p_{\text{perfect capsid}}^{-1/N} - 1 \right) \tag{21}$$

Figure 6 shows plots of this expression in the (N, k) plane for $p_{\text{perfect capsid}} = 0.99$ and $p_{\text{perfect capsid}} = 0.95$, along with values of N and k for several viruses. The formation of defective capsids is easiest (the threshold value of $\Delta\Delta G$ needed for the formation of defective capsids is least) for viruses with a large number of subunit in which each subunit has few neighbors, whereas it is hardest to form defects in viruses with few subunits in which each subunit has many neighbors.

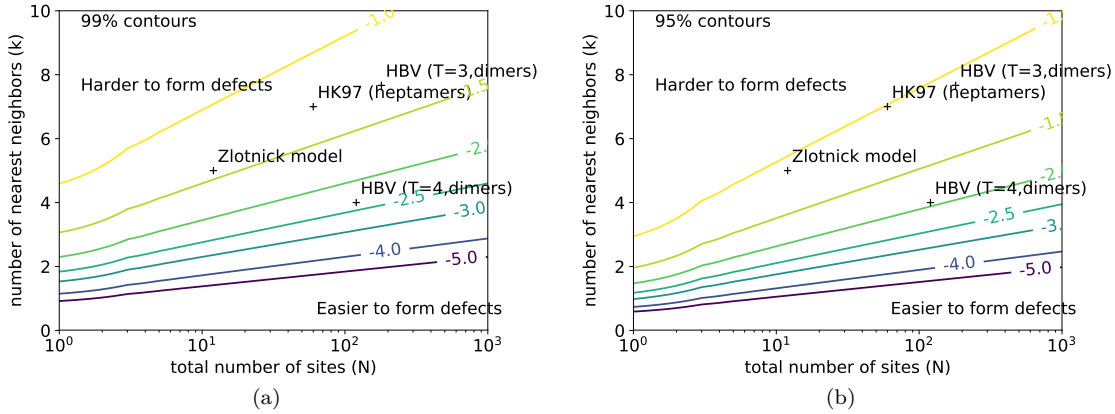

Figure 6: Summary plot for arbitrary spherical viruses. Dependence of the threshold value of $\Delta\Delta G$ needed to ensure a high proportion of capsid formation on the total number of subunits in the capsid N and the number of nearest neighbors k, based on equation 21. (a) 99% capsid formation; (b) 95% capsid formation. Values of N and k for selected viruses are plotted as well.

5 Discussion

5.1 Comparison with prior work

Our model, while still greatly simplified, improves over prior theoretical work in several ways. Generally speaking, our model incorporates more realistic and combinatoric possibilities than the seminal early model of Zlotnick [26]. We also find two-state behavior – mostly assembled and mostly disassembled – but the greater granularity of our model clearly shows that what appeared to be a uniform assembled state in the prior work consists of an *ensemble* of nearly fully assembled configurations in large parts of parameter space. That is, defects are common, both as vacancies and/or mis-assembled sites.

A model somewhat similar to ours has been used to study the assembly of CCMV.[30, 31] This model incorporates a grand-canonical term and a hydrophobic interaction term with the same forms as the two terms in equation 20. Unlike our model, they consider only vacant and ideally occupied sites and do not consider mis-occupied sites. In addition, unlike our model, this model includes an explicit Debye-Huckel electrostatic term dependent on the distances between subunit sites, whereas in our model, both hydrophobic and electrostatic interactions are included in the ΔG_{ideal} and ΔG_{defect} parameters. Although the electrostatic term in principle includes interactions between any pair of sites, not just those that are in contact, it is likely that at moderate ionic strength, non-contact interactions are very limited because the distance between subunits in a viral capsid is typically much greater than the Debye-Huckel screening length. Thus, this model and ours are likely to exhibit similar mathematical behavior, and in fact the model produces distributions of capsid sizes that are two-peaked with the higher peak not being at full assembly, similar to those shown in figure 4 for our model. It is also worth noting that, while CCMV subunits have a negatively charged exterior and positively charged interior,[8] HBV subunits have a more complex charge distribution, so there may be a larger role for electrostatics in CCMV assembly compared to HBV assembly. Nevertheless, the use of an explicit electrostatic term allows for an analysis of the explicit dependence of capsid assembly on temperature, ionic strength, and pH.

In experimental studies of hepatitis B viral capsid assembly, only two populations were observed using size-exclusion chromatography. Their molecular weights were measured using light scattering and corresponded to complete capsids and free dimers.[29] This is broadly consistent with our Monte Carlo simulations, which in most cases produce capsid size distributions peaked around either 1 dimer or 120 dimers, corresponding to a free dimer or a complete capsid respectively. In a few cases we observe a distribution containing peaks corresponding to both sizes. The observation of only two peaks would seem to rule out significant concentrations of defective or partially assembled capsids. However, the experimental data is not sufficient to support this conclusion, because size-exclusion chromatography relies on hydrodynamic volume, not molecular weight, to resolve macromolecules,[37] and capsids with localized defects (such as missing dimers) would be expected to have a hydrodynamic volume very close to those of perfect capsids. Furthermore, the theory of light scattering is based on the assumption that the biomolecular particles detected are spherical with a refractive index that differs slightly from that of the surrounding medium.[38] Consequently, the observed population corresponding to complete capsids may also include defective capsids that are nearly complete – i.e., species which may be of great biological importance.

5.2 Limitations of our model and avenues for future improvement

One limitation of the statistical-mechanical model described here is that it considers the formation of only one capsid at a time, from a gas of free subunits. The possible defects are limited to vacant sites or sites with partially attached subunits. In other simulations, using structurally more realistic models, more complex structures were formed. For example, the Brooks group obtained a variety of irregular capsids, including twisted, tubular, prolate and conical capsids, as well as partially formed capsids with missing subunits and open misaggregates consisting of two partial capsids joined together.[22, 23] It is not obvious how to extend a model of the type presented here to accommodate irregular capsids or misaggregates.

Another limitation is ambiguity in the physical interpretation of the four free parameters, the chemical potential of free subunits μ and three interaction strengths: ΔG_{ideal} between fully occupied subunits, ΔG_{mixed} between fully-occupied and mis-occupied subunits, and ΔG_{defect} between mis-occupied subunits. a Since μ is the chemical potential of free subunits with which we are assuming the partially formed capsid is

in equilibrium, it is related to an effective concentration of free subunits via equation 4. However, it is not clear what the the reference concentration $[\text{subunit}]_{\text{ref}}$ should be in this setting.

The parameter ΔG_{ideal}, the interaction free energy, must include all environmental factors, including temperature and ionic strength. The experimental values for the interaction strength among human hepatitis B subunits range from approximately -3.2 to -4.4 kcal/mol,[29] which correspond to values of ΔG_{ideal} from approximately -5 to -7 $k_B T$, on the upper end of the values considered here. The lower values are more consistent with physiological conditions; the strength of the intersubunit interaction increases with increasing temperature and ionic strength. Experimental studies comparing woodchuck and human HBV also demonstrate that the two proteins, despite having approximately 65% sequence identity and forming very similar assembled capsid structures, have very different thermodynamics of assembly, with woodchuck HBV having a stronger entropic contribution to assembly.[39] In previous simulations (including our own), stronger interactions are usually used in order to speed up capsid formation. In the simulations performed by Hagan and Chandler, a "hysteresis" effect was observed[24] in which it was necessary to use a somewhat smaller interaction strength (about $12k_B T$) to cause fully assembled capsids to disassemble, compared to the interaction strength needed to assemble capsids from free subunits (about $16k_B T$). In our own simulations,[25] the energy of an intersubunit interaction is about 8 kcal/mol per intersubunit interaction, or about $13.3k_B T$ where $T = 300$ K is the simulation temperature.

6 Conclusions

To investigate systematically the potential for defect formation in virus capsids, we developed a statistical mechanical model that incorporates more realistic capsid geometry than prior work, as well as taking into account the possibility of weaker intersubunit interactions due to partial attachment of subunits. Both analytical approximations and Monte Carlo simulations reveal that significant proportions of defective capsids can form when the difference in strengths between ideal and defective subunits is below a threshold, which depends only on geometric properties of the capsid. While significant work remains to be done in extending the model to allow a greater variety of defects, and in clarifying the physical meaning of the parameters, these results demonstrate that the concentration of defective capsids can be more significant under certain conditions than previously appreciated.

7 Acknowledgments

We thank Dr. David Koes, Dr. Lillian Chong, Barmak Mostofian, and Jeremy Copperman for helpful discussions and technical assistance. We also thank the Advanced Computing Center at OHSU for computer time. This work was supported by NIH grants 1R01-GM115805 and R21-AI130745, and by NSF grants MCB-1715823 and CNS-1229064.

References

[1] Jason D. Perlmutter and Michael F. Hagan. Mechanisms of virus assembly. *Annu. Rev. Phys. Chem.*, 66:217–39, 2015.

[2] Mauricio G. Mateu. Assembly, stability and dynamics of virus capsids. *Arch. Biochem. Biophys.*, 531: 65–79, 2013.

[3] W. Gibson and B. Roizman. Proteins specified by herpes-simplex virus .8. characterization and composition of multiple capsid forms of subtypes 1 and 2. *J. Virol.*, 10(5):1044–1052, 1972.

[4] F. L. Homa, J. B. Huffman, K. Toropova, H. R. Lopez, A. M. Makhov, and J. F. Conway. Structure of the pseudorabies virus capsid: Comparison with herpes simplex virus type 1 and differential binding of essential minor proteins. *J. Mol. Biol.*, 425(18):3415–3428, 2013.

[5] A. Zlotnick, N. Cheng, J. F. Conway, F. P. Booy, A. C. Steven, S. J. Stahl, and P. T. Wingfield. Dimorphism of hepatitis b virus capsids is strongly influenced by the c-terminus of the capsid protein. *Biochemistry*, 35(23):7412–7421, 1996.

[6] N. R. Watts, J. F. Conway, N. Q. Cheng, S. J. Stahl, D. M. Belnap, A. C. Steven, and P. T. Wingfield. The morphogenic linker peptide of hbv capsid protein forms a mobile array on the interior surface. *EMBO J.*, 21(5):876–884, 2002.

[7] M. A. DiMattia, N. R. Watts, S. J. Stahl, J. M. Grimes, A. C. Steven, D. I. Stuart, and P. T. Wingfield. Antigenic switching of hepatitis b virus by alternative dimerization of the capsid protein. *Structure*, 21 (1):133–142, 2013.

[8] L. Lavelle, M. Gingery, M. Phillips, W. M. Gelbart, C. M. Knobler, R. D. Cadena-Nava, J. R. Vega-Acosta, L. A. Pinedo-Torres, and J. Ruiz-Garcia. Phase diagram of self-assembled viral capsid protein polymorphs. *J. Phys. Chem. B*, 113(12):3813–3819, 2009.

[9] J. Chang, X. A. Liu, R. H. Rochat, M. L. Baker, and W. Chiu. *Reconstructing Virus Structures from Nanometer to Near-Atomic Resolutions with Cryo-Electron Microscopy and Tomography*, volume 726 of *Advances in Experimental Medicine and Biology*, pages 49–90. Springer-Verlag Berlin, Berlin, 2012. ISI Document Delivery No.: BZG80 Times Cited: 16 Cited Reference Count: 180 Chang, Juan Liu, Xiangan Rochat, Ryan H. Baker, Matthew L. Chiu, Wah Article; Book Chapter HEIDELBERGER PLATZ 3, D-14197 BERLIN, GERMANY.

[10] D. Veesler, B. M. Kearney, and J. E. Johnson. Integration of x-ray crystallography and electron cryo-microscopy in the analysis of virus structure and function. *Crystallogr. Rev*, 22(2):102–127, 2016.

[11] James F. Conway, N. Cheng, Adam Zlotnick, P. T. Wingfield, S. J. Stahl, and A. C. Steven. Visualization of a 4-helix bundle in the hepatitis b virus capsid by cryo-electron microscopy. *Nature*, 386(6620):91–94, 1997.

[12] Gale Rhodes. *Crystallography made Crystal Clear, 3rd ed.* Elsevier Academic Press, 2006.

[13] E. Nogales and S. H. W. Scheres. Cryo-em: A unique tool for the visualization of macromolecular complexity. *Mol. Cell*, 58(4):677–689, 2015.

[14] Y. Cheng, N. Grigorieff, P. A. Penczek, and T. Walz. A primer to single-particle cryo-electron microscopy. *Cell*, 161(3):438–449, 2015.

[15] James F. Conway and Alasdair C. Steven. Methods for reconstructing density maps of "single" particles from cryoelectron micrographs to subnanometer resolution. *Journal of Structural Biology*, 128(1):106–118, 1999.

[16] Russell Schwartz, Peter W. Shor, Jr. Peter E. Prevelige, and Bonnie Berger. Local rules simulation of the kinetics of virus capsid self-assembly. *Biophysical Journal*, 75:2626–2636, 1998.

[17] Johanna E. Baschek, Heinrich C. R. Klein, and Ulrich S. Schwarz. Stochastic dynamics of virus capsid formation: direct versus hierarchical self-assembly. *BMC Biophysics*, 5, 2012.

[18] Lu Xie, Gregory R. Smith, Xian Feng, and Russell Schwartz. Surveying capsid assembly pathways through simulation-based data fitting. *Biophysical Journal*, 103:1545–1554, 2012.

[19] Matthew R. Perkett and Michael F. Hagan. Using markov state models to study self-assembly. *J. Chem. Phys.*, 140:214101, 2014.

[20] Eric C. Dykeman, Peter G. Stockley, and Reidun Twarock. Solving a levinthal's paradox for virus assembly identifies a unique antiviral strategy. *Proc. Natl. Acad. Sci. USA*, 111(14):5361–5366, 2014.

[21] Hung D. Nguyen, Vijay S. Reddy, and Charles L. Brooks III. Deciphering the kinetic mechanism of spontaneous self-assembly of icosahedral capsids. *Nano Lett.*, 7(2):338–344, 2007.

[22] Hung D. Nguyen and Charles L. Brooks III. Generalized structural polymorphism in self-assembled viral particles. *Nano Lett.*, 8(12):4574–4581, 2008.

[23] Hung D. Nguyen, Vijay S. Reddy, and Charles L. Brooks III. Invariant polymorphism in virus capsid assembly. *J. Am. Chem. Soc.*, 131:2606–2614, 2009.

[24] Michael F. Hagan and David Chandler. Dynamic pathways for viral capsid assembly. *Biophysical Journal*, 91:42–54, 2006.

[25] Justin Spiriti and Daniel M. Zuckerman. Tabulation as a high-resolution alternative to coarse-graining protein interactions: Initial application to virus capsid subunits. *J. Chem. Phys.*, 143:243159, 2015.

[26] A. Zlotnick. To build a virus capsid - an equilibrium-model of the self-assembly of polyhedral protein complexes. *J. Mol. Biol.*, 241(1):59–67, 1994.

[27] R. F. Bruinsma and W. S. Klug. Physics of viral shells. *Annual Review of Condensed Matter Physics, Vol 6*, 6:245–268, 2015.

[28] Adam Zlotnick, Jennifer M. Johnson, Paul W. Wingfield, Stephen J. Stahl, and Dan Endres. A theoretical model successfully identifies features of hepatitis b virus capsid assembly. *Biochemistry*, 38(44): 14644–14652, 1999.

[29] Pablo Ceres and Adam Zlotnick. Weak protein-protein interactions are sufficient to drive assembly of hepatitis b virus capsids. *Biochemistry*, 41(39):11525–11531, 2002.

[30] J. Z. Chen, M. Chevreuil, S. Combet, Y. Lansac, and G. Tresset. Investigating the thermal dissociation of viral capsid by lattice model. *J. Phys.-Condes. Matter*, 29(47):8, 2017.

[31] G. Tresset, J. Z. Chen, M. Chevreuil, N. Nhiri, E. Jacquet, and Y. Lansac. Two-dimensional phase transition of viral capsid gives insights into subunit interactions. *Phys. Rev. Appl.*, 7(1):8, 2017.

[32] David Chandler. *Introduction to Modern Statistical Mechanics*. Oxford University Press, USA, 1987.

[33] R. K. Pathria. *Statistical Mechanics*. Elsevier, Amsterdam, 1996.

[34] N. Metropolis, A. W. Rosenbluth, M. N. Rosenbluth, A. H. Teller, and E. Teller. Equation of state calculations by fast computing machines. *J. Chem. Phys.*, 21(6):1087–1092, 1953.

[35] Daniel M. Zuckerman. *Statistical Physics of Biomolecules: An Introduction*. CRC Press, Boca Raton, FL, 2010.

[36] S. A. Wynne, R. A. Crowther, and A. G. W. Leslie. The crystal structure of the human hepatitis b virus capsid. *Mol. Cell*, 3(6):771–780, 1999.

[37] Michael Eisenstein. Adventures in the matrix. *Nat. Methods*, 3:410, 2006.

[38] Bruno H. Zimm. Apparatus and methods for measurement and interpretation of the angular variation of light scattering; preliminary results on polystyrene solutions. *The Journal of Chemical Physics*, 16 (12):1099–1116, 1948.

[39] A. A. Kukreja, J. C. Y. Wang, E. Pierson, D. Z. Keifer, L. Selzer, Z. Tan, B. Dragnea, M. F. Jarrold, and A. Zlotnick. Structurally similar woodchuck and human hepadnavirus core proteins have distinctly different temperature dependences of assembly. *J. Virol.*, 88(24):14105–14115, 2014.